

Article

Characterization of Ancient Mortars from Minoan City of Kommos in Crete

Pagona-Noni Maravelaki ^{1,*} , Antonis Theologitis ¹, Meral Budak Unaler ¹, Chrysi Kapridaki ¹ ,
Kali Kapetanaki ¹  and James Wright ²

¹ School of Architecture, Technical University of Crete, Akrotiri, 73100 Chania, Greece; theologitis@gmail.com (A.T.); meralbudak@gmail.com (M.B.U.); ckapridaki@gmail.com (C.K.); kkapetanaki@isc.tuc.gr (K.K.)

² American School of Classical Studies, 10676 Athens, Greece; jwright@brynmaur.edu

* Correspondence: pmaravelaki@isc.tuc.gr

Abstract: This work characterizes ancient mortars used in construction of the Bronze Age Minoan port at Kommos in Crete. The port dates from c. 1850 BCE with port facilities at the harbor and residences on the Central hillside and the Hilltop. A Greek, Phoenician, and Roman sanctuary overlies the administrative center. The first step collected representative samples from the different construction phases, previous conservation interventions, exposure to different environmental factors, and different material composition. From these 10 mortar samples were analyzed using stereo- and digital microscopy, X-ray diffraction (XRD), X-ray Fluorescence (XRF), and Fourier Transform Infrared spectroscopy (FTIR) to determine texture, morphology, mineralogical, and physico-chemical properties. The physico-chemical and mineralogical analyses divided the samples into two groups: lime binder mortars and earthen binder mortars. The main minerals identified in the samples are calcite, quartz, dolomite, illite, albite, kaolinite, and vermiculite. Analysis of local clay showed that local materials were used in the production of these mortars. The analysis of mortar samples with stereomicroscopy, XRF, and FTIR showed that the samples are mainly composed of calcite and silicates in major quantities along with aluminum, magnesium, and iron oxide in minor quantities. A wide variety of local aggregates and ceramic fragments were used in the production of these ancient mortars. The mortar condition resulted in a decay state that needs conservation interventions. This characterization of the ancient mortars was important for the design of compatible restoration mortars.

Keywords: Kommos ancient mortars; physico-chemical and mineralogical analyses; earthen and lime mortars



Citation: Maravelaki, P.-N.; Theologitis, A.; Budak Unaler, M.; Kapridaki, C.; Kapetanaki, K.; Wright, J. Characterization of Ancient Mortars from Minoan City of Kommos in Crete. *Heritage* **2021**, *4*, 3908–3918. <https://doi.org/10.3390/heritage4040214>

Academic Editors:
Antonia Moropoulou,
Elisabetta Zendri, Ekaterini Deleogou
and Michael Turner

Received: 31 August 2021
Accepted: 15 October 2021
Published: 22 October 2021

Publisher's Note: MDPI stays neutral with regard to jurisdictional claims in published maps and institutional affiliations.



Copyright: © 2021 by the authors. Licensee MDPI, Basel, Switzerland. This article is an open access article distributed under the terms and conditions of the Creative Commons Attribution (CC BY) license (<https://creativecommons.org/licenses/by/4.0/>).

1. Introduction

The archaeological site of Kommos is located in the province of Heraklion, five kilometers southwest of the Bronze Age palace at Phaistos, Crete. The site was excavated in the years 1976–1996 by Professors Joseph and Maria Shaw of the University of Toronto under the auspices of the American School of Classical Studies [1–9]. Located on the shore of the Libyan Gulf, Kommos was the port of Phaistos. Kommos was established c. 1850 BCE and flourished throughout the Minoan period until it was abandoned about 1200 BCE. A small port town grew up around a cluster of major administrative, industrial, and storage buildings that served the boats that plied the trade routes of the Eastern Mediterranean. Kommos actively traded with Sardinia, southern Italy, the Greek Mainland, the Aegean islands, Cyprus, Anatolia, the Levantine coast, and Egypt, while the evidence from the sanctuary shows that both Greeks and Phoenicians worshipped there [10].

In 2016 a project for the protection of the ruins at Kommos began in collaboration with the Laboratory of Materials for Cultural Heritage & Modern Building (MaCHMoB) of the Technical University of Crete and the University of Toronto Excavations at Kommos.

A master plan for conservation of the ruins at Kommos identified major factors affecting the preservation of the standing remains, among them sea aerosols, standing water, wind, and invasive plants. A first priority was to stabilize the standing remains, many of which were severely eroded and in danger of collapse. Assessment of the ancient mortars was necessary to identify their composition, their technical deployment, and their performance over the centuries of exposure. This assessment guided the design of replacement mortars to ensure their visual and mechanical compatibility with the ancient ones.

The characterization of the ancient mortars focused on their mineralogical composition and physico-chemical properties [11–16]. Such a process of reverse engineering produces recipes that are compatible with the local conditions and materials, and ensure the long viability of modern interventions. As is well known, the usage of incompatible materials can cause irreversible damage to ancient structures in need of conservation [17,18].

Therefore, 45 samples were collected at Kommos, of which 10 were selected as representative for this presentation. These include samples from the different historic periods and locations at the site. They clarify the technology of preparation, composition, and nature of mortars that provide guidelines for the design of compatible and well-performing conservation mortars.

2. Sampling and Experimental Procedure

2.1. Sampling

The port at Kommos consists of the prehistoric Civic Center of the harbor area, over which is the Greek Sanctuary, and the town up slope to the north divided into the Central Hillside and the Hilltop Houses (Figure 1). The Bronze Age port facilities and town belong to the Middle through Late Bronze Ages (c. 1850–1200 BCE) while the sanctuary extends from c. 1025 BCE into the second century CE of the Roman era. For this study the mortar samples correspond to the following criteria: chronological, structural, corrosion, and macroscopic characteristics (Table 1). Attention was paid to sampling from the upper part of the buildings to avoid decay patterns due to the capillary rise.

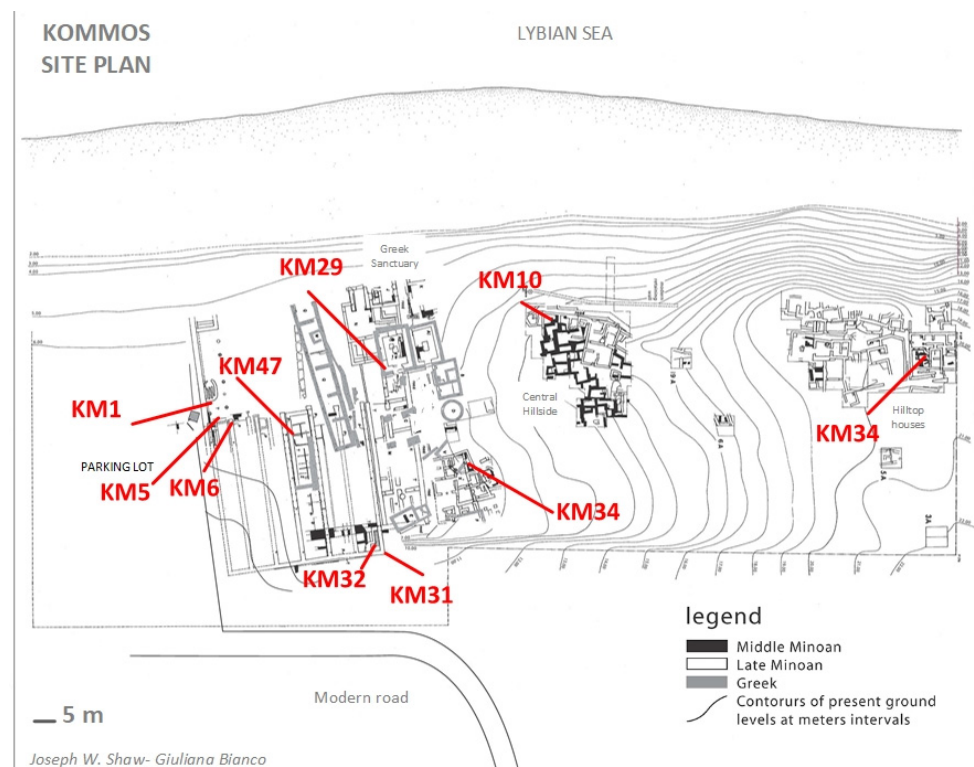


Figure 1. Sampling points of mortar samples on map.

Table 1. Sampling data of the mortars.

Sample Name	Location	Function	Period
KM1	Civic Center, South Stoa	Pointing Mortar	Bronze Age
KM5	Civic Center, South Stoa	Pointing Mortar	Bronze Age
KM6	Civic Center, South Stoa	Joint Mortar	Bronze Age
KM10	Central Hillside	Joint Mortar	Late Minoan
KM29	Greek Sanctuary	Joint Mortar	Late Minoan
KM31	Greek Sanctuary	Joint Mortar	Late Bronze Age
KM32	House X	Joint Mortar	Late Bronze Age
KM34	House X	Joint Mortar	Late Bronze Age
KM42	Hilltop Houses	Pointing Mortar	Middle Minoan
KM47	Building P	Pointing Mortar	Late Bronze Age

2.2. Experimental

The samples were first studied macroscopically, followed by a systematic stereo- and digital microscopic; a chemical and mineralogical study followed with the aid of appropriate analytical techniques.

In order to obtain information about components of the mortar samples, and the binder to aggregates ratio, the samples were fractionated and sieved through an ISO 565 series of sieves. This provided better identification of the different mineralogical phases. The lowest fraction, which was $<63 \mu\text{m}$, was mostly attributed to the binder. Sometimes fine grained aggregates could be detected in this fraction [19,20].

The crystalline phases in the mortars were characterized by X-Ray Diffraction analysis performed with a Siemens D-500 diffractometer working with Cu K α radiation ($\lambda = 1.5418 \text{ \AA}$) and by a graphite monochromator in a diffracted beam at 1.5 kW. XRD patterns were taken from 4° to 60° 2θ at about 1.8° $2\theta/\text{min}$ (step size = 0.03° 2θ ; time = 1 s).

Infrared spectroscopy (FTIR, Perkin-Elmer 1000) was used to obtain qualitative chemical information on some of the characteristic compounds contained in mortar (calcium and magnesium hydroxides, carbonates, gypsum, etc.) and for determining the presence of salts (nitrates, sulfates, oxalates, etc.), as well as organic compounds [21]. The FTIR spectra were acquired in transmission mode on KBr pellets of samples and converted to absorbance mode covering the wave number range of $400\text{--}4000 \text{ cm}^{-1}$ with a resolution of 4 cm^{-1} . In order to obtain good signal to noise ratio, 20 consecutive scans were added and averaged before Fourier transform. In this study, powders from the fine fraction of samples ($<63 \mu\text{m}$), mostly representing the binder, were used to elucidate the binder composition and discover the presence of clay minerals [20].

Stereo- and digital microscopy was used to obtain information about the microstructure of the samples, the binder-to-aggregate adhesion, and the grain size distribution. Fine polished cross-sections were prepared for the samples whenever it was considered necessary to further elaborate the microstructural features.

The Energy Dispersive X-Rays Fluorescence (EDXRF) with ^{109}Cd and ^{55}Fe radioactive sources, a silicon drift detector (SDD), with Peltier cooling (-25°C , no liquid nitrogen), and an $8 \mu\text{m}$ Moxtek Dura-Be window, resolution 150 eV at 5.9 keV, TC-244 Spectroscopy Amplifier, PCA-II Nucleus Multichannel card, AXIL (RN) computer program analysis were employed for qualitative and quantitative analyses of the samples; the most appropriate quantification was applied and checked on standard samples [22]. The measurements were directly performed on the fine-grained powders of the samples at 40 kV and 0.9 mA, in ambient air or with Helium gas flushing, using a 12-position automatic sampler. The irradiation time was 300 s (5 min).

3. Results and Discussion

3.1. Macroscopic and Stereomicroscopic Analyses

The macroscopic analysis of samples showed that the majority of the samples showed a light gray-brown color, especially where lime was mixed with earthen material and sand.

A crust due to biological agents was detected on the surface. In some samples, crushed ceramic fragments, fibers, hairs, and marine shells were detected. All the samples were very fragile (Figure 2).

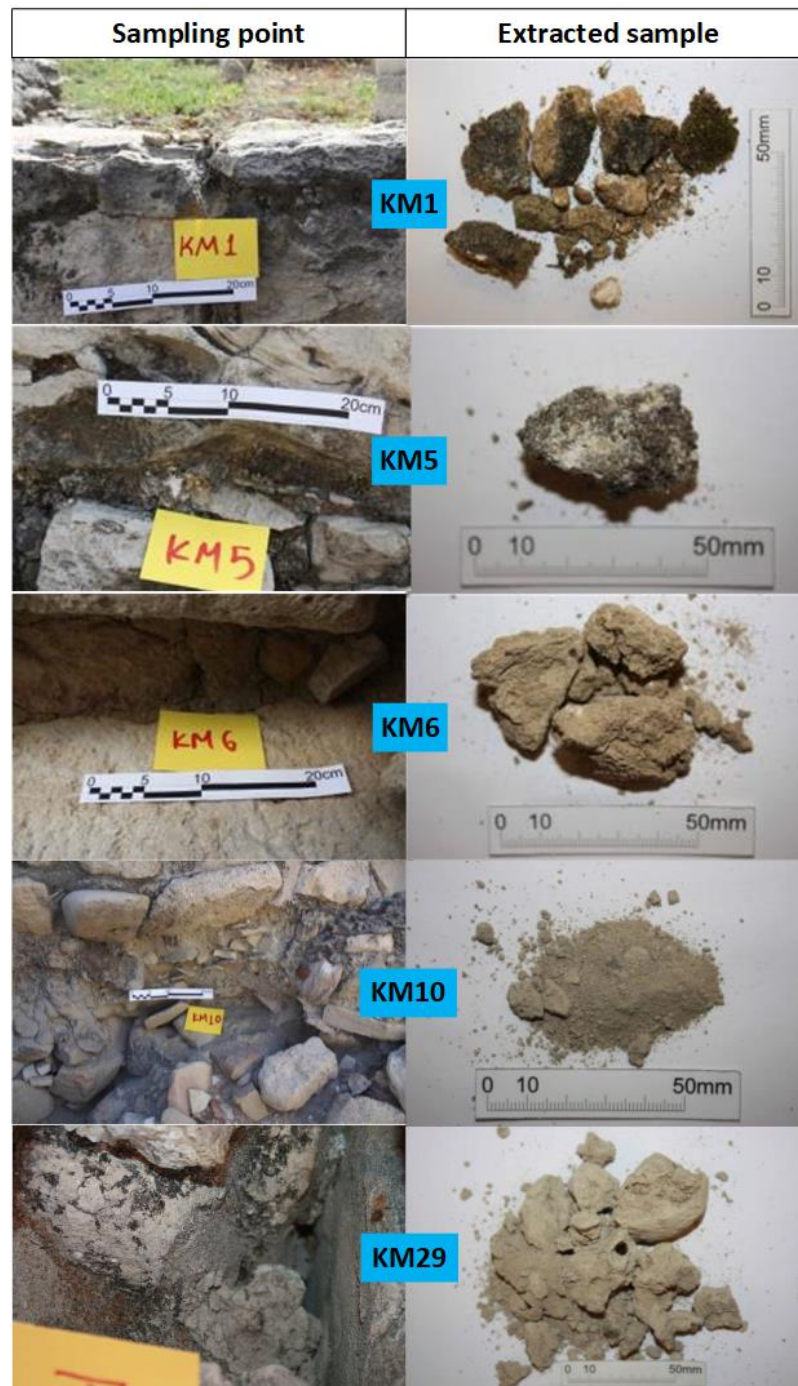


Figure 2. Sampling points and macrophotographs of samples.

Stereomicroscopic analysis of polished cross sections of the samples provided information about general characteristics such as color, microstructure, type of mortar, and aggregates (Figure 3). According to the results, sample surfaces were covered by a layer of biological sediments (black spots) on outside. The calcite content detected in samples was considerable. The most important finding was the presence of animal fibers (up to 5 mm) in the mortars. Sea sand (up to 2 mm) or river sand (1.5 mm) were also used as aggregates.

These mortars contained ceramic fragments of 800 μm in diameter, and marine shells up to 10 mm; microcracks and calcite grains were also observed in the mortar structure.

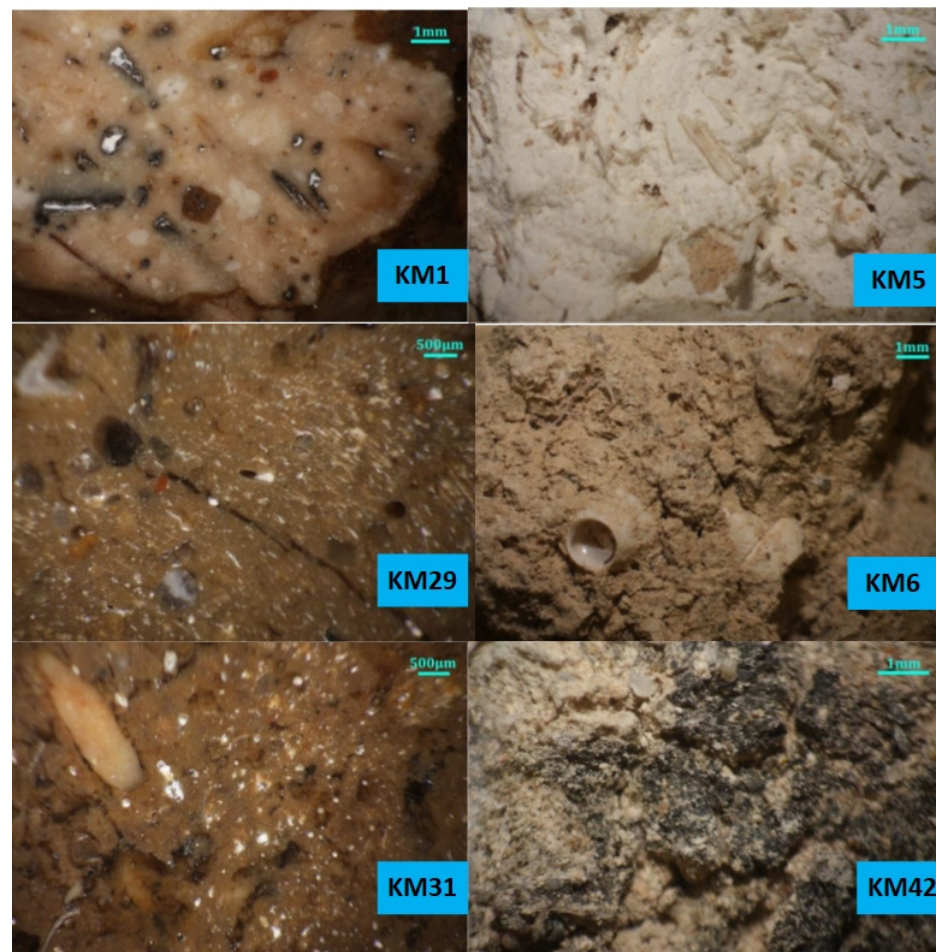


Figure 3. Stereomicroscopy microphotographs in different magnifications of polished sections (KM1, KM29, KM31) and samples (KM5, KM6, KM42).

Examination of the microstructure of samples, however, demonstrated a durable, solid mortar with a negligible degree of wear. These mortars contained binders of clay and lime, differing in the binder and/or aggregate content. Many of them contained straw as an inert, a technique widely used in antiquity [23]. Characteristics of samples determined by stereomicroscopic analysis are given in Table 2.

In accordance with the original examination of the mortars, two primary groups were recognized: those in which earthen material was used as binder (KM6, KM10, KM29, KM31, KM34, KM42, KM47) and those with a lime binder (KM1, KM5). The second group consisted largely of calcite, as identifiable by color and a very fine sand aggregates, and fibers (straw), which was a very common practice in prehistoric and historic times. These samples also included sparse ceramic fragments, a common practice found in mortars and mudbrick [23].

The rest of the mortars were earthen mortars with sea sand as aggregates. Sea shells of differing quantity and size were also identified in the mortars' structure. Their presence could either be coincidental due to the use of sea sand or intentional. For example, in the sampling point of KM10 and elsewhere at the site, lots of sea shells were noticed among the ruined structures. Even though their binder was mainly clay, on some occasions lime has been used in small quantities. This was attributed to the sporadic presence of calcite conglomerates in some samples (e.g., see Figure 3, KM6) and to some whitish spots observed in the cross-section of sample KM29.

Table 2. Characteristics of samples.

Samples	Characteristics
KM1	Intense white color, binder rich in lime, presence of straw fibers
KM5	Intense white color, binder rich in lime, presence of straw fibers
KM6	Earthen binder, coarse microstructure, sea shells, cracks
KM10	Earthen binder, poor performance, many sea shells
KM29	Earthen binder, very fine inert
KM31	Earthen binder, coarse microstructure, sea shells, voids and cracks
KM32	Earthen binder, sea sand, sea shells
KM34	Earthen binder, well performing mortar
KM42	Earthen binder, mortar with poor performance, many sea shells
KM47	Earthen binder, fine sea sand, sporadic sea shells

The microstructure of mortars was differentiated under the stereomicroscope observations as can be clearly seen in Figure 3. Most of the Bronze Age Minoan mortars from the south area showed an advanced deteriorated microstructure characterized by micro-cracks (KM31). However, these micro-cracks were mostly very fine, producing only moderate damage to the whole structure. Those micro-cracks and voids that were observed in the structure resulted from the aging and leaching of mortar because of environmental loading and highlight the necessity of conservation to preserve the structures. The same observation applies to the Bronze Age Minoan mortars from the Central Hillside and Hilltop areas. The microstructure of sample KM29 was quite different: it was characterized by very fine granules (both binder and aggregate) and much more compactness, without most of the cracking or voids.

3.2. XRD Analysis

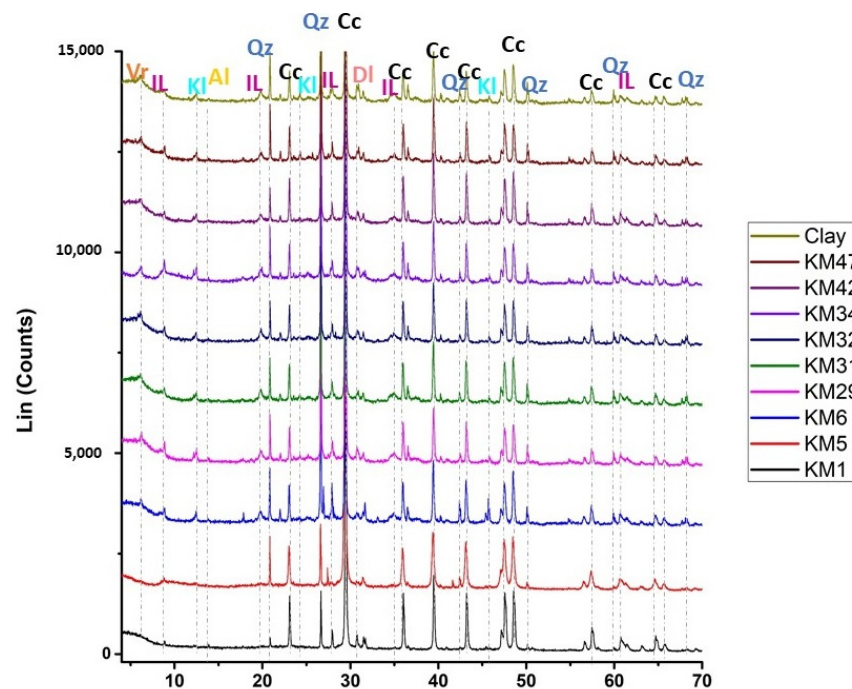
The results of X-ray diffraction analysis are given in Table 3 and the corresponding patterns are presented in Figure 4. According to the results, all samples contained silicate (quartz, illite, kaolinite, corrensite, epidote and montmorillonite), carbonate (calcite, dolomite and aragonite), and feldspar (albite, anorthite, and orthoclase) minerals in their structure in varying amounts [24]. The KM Clay sample was rich in calcite, with clay minerals such as illite, kaolinite, vermiculite, montmorillonite, and albite, with high amounts of quartz contrasted with low amounts of dolomite.

Quartz (SiO_2), calcite CaCO_3 , illite ($\text{KAl}_2\text{Si}_3\text{AlO}_{10}(\text{OH})_2$), and kaolinite ($\text{Al}_2\text{Si}_2\text{O}_5(\text{OH})_4$) were the most common minerals in each mortar samples. These samples were very rich in calcite, because of the content of lime in their structure. Calcite is the most stable member of the calcium carbonate family and the most common form of calcium carbonate found in archaeological sites. The origin of calcite can be biogenic, geogenic, or pyrogenic [25,26]. A biogenic calcite source is bird eggshells and mollusk shells. Calcite can also be formed from sea water but this calcite contains a large amount of magnesium in its structure [27].

Aragonite is the second most common form of calcium carbonate [28]. Aragonite is one of the metastable polymorphs of calcium carbonate at ambient temperature and pressure [29]. Generally, the aragonite found in archaeological sites is biogenic-derived from the shells of terrestrial gastropods, freshwater bivalves, and marine mollusks [27,29,30]. In archaeological sites, aragonitic shells are very commonly found [31,32]. If the shell is still preserved as aragonite, it can be said that the preservation conditions are relatively good [27]. Aragonite also precipitates out of evaporating seawater at ambient temperatures and pressures. Sea water includes Mg ions in its structure, which prevents calcite nucleation and results in aragonite forms. Thus the presence of aragonite in mortar samples could be also indicative of a marine environment [27]. Aragonite was detected in structures of all the samples except for KM29 and KM42.

Table 3. Mineralogical composition of samples.

XRD	Mineralogical Composition
KM1	calcite, quartz, illite, kaolinite, dolomite, anorthite, aragonite, orthoclase, halite
KM5	calcite, quartz, illite, dolomite, orthoclase, halite,
KM6	calcite, quartz, illite, kaolinite, dolomite, anorthite, aragonite, halite, corrensite
KM10	calcite, quartz, illite, kaolinite, albite, aragonite, epidote, halite, halite, montmorillonite
KM29	calcite, quartz, illite, kaolinite, dolomite, albite, epidote, lizardite, vermiculite
KM31	calcite, quartz, illite, kaolinite, dolomite, albite, aragonite, lizardite, vermiculite
KM32	calcite, quartz, illite, kaolinite, albite, aragonite, epidote, lizardite, vermiculite
KM34	calcite, quartz, illite, kaolinite, dolomite, albite, aragonite, epidote, lizardite, vermiculite
KM42	calcite, quartz, illite, kaolinite, dolomite, albite, lizardite, vermiculite
KM47	calcite, quartz, illite, kaolinite, dolomite, albite calcian, aragonite, lizardite, vermiculite
KM Clay	calcite, quartz, illite, kaolinite, dolomite, albite, vermiculite, montmorillonite

**Figure 4.** XRD patterns of samples with the main minerals; Cc: calcite, Qz: quartz, IL: illite, Al: albite, Kl: kaolinite, Vr: vermiculite.

Dolomite also appears as integral constituent of the lime binder, whereas quartz was present as a residue of the inert aggregates, when passed through the 63 μm sieve. Kaolinite could not be detected in the matrix of Sample KM5. This sample was a lime mortar prepared with a high amount of lime, very fine sand aggregate, fibers (straw), and ceramic fragments. Absence of kaolinite in the matrix could be proof of the clay calcination occurring during ceramic production.

Dolomite could not be identified in samples KM10 and KM32. Dolomite was an integral constituent of the lime binder. The absence of dolomite in these samples can be explained by the use of lime and/or earthen material originating from different sources. All of the mortars contained local argillaceous earth. Consequently, the XRD patterns were very similar and to the XRD pattern of KM clay. This revealed the constant use of local earth material throughout the history of the site. The diffractographs of the mortar samples exhibited slightly higher peaks for calcite and quartz and showed also some peaks of other minerals (epidote, lizardite), all attributed to the inert material. Halite in the mortar

structures originates from the use of coastal sand for production. The presence of halite is also evidence of salt crystallization [33].

3.3. XRF Analyses

XRF analyses of the samples are given in Table 4. Results show that CaO and SiO₂ are the main chemical constituents of samples. CaO is the main component of the mortars with concentration ranges between 29–48 wt%, whereas SiO₂ ranges between 7–30 wt%. The quantity of SiO₂ in mortar samples is related to the presence of siliceous sand, clay and ceramic aggregates in the mortars. The percentage of MgO observed in the samples ranges between 2–5 wt%. Alumina content of the samples is between 2–8 wt%. The identification of high concentration of SiO₂ and Al₂O₃ could be related to the addition of aggregate and clay in mortar. SO₃ concentrations are lower than 0.2 wt%. Most probably, part of the analyzed samples originates from external decayed parts of the structures, which suffer from the marine aerosols more than the interior part. The high content of MgO (2.2–4.5 wt%) reflects the presence of dolomite, as evidenced by both XRD and FTIR analyses. The Na₂O concentration of samples reach values up to 2.5 wt%; this is expected from the marine context of the site and the consequent decay state. XRF results corroborate the results of the XRD analysis.

Table 4. Chemical composition of samples (wt%) identified by XRF.

XRF	KM1	KM5	KM6	KM10	KM29	KM31	KM32	KM34	KM42	KM47	KM Clay
CaO	41.01	47.55	32.53	34.99	29.97	30.74	30.56	30.85	37.18	32.38	29.18
SiO ₂	17.32	7.17	27.85	26.77	30.37	29.06	29.49	27.16	22.82	28.02	28.21
Al ₂ O ₃	3.75	1.58	7.58	5.84	7.93	7.51	7.66	7.07	5.62	7.15	7.25
MgO	2.80	2.15	4.46	4.03	4.34	3.59	4.03	4.37	3.36	4.14	4.19
Fe ₂ O ₃	2.14	1.11	4.08	3.12	4.27	4.09	4.20	4.07	3.32	4.06	3.86
Na ₂ O	1.01	1.51	2.50	1.63	1.56	1.13	1.06	1.79	0.93	1.10	1.81
K ₂ O	0.59	0.26	1.24	0.98	1.43	1.28	1.27	1.26	1.01	1.26	1.24
SO ₃	0.19	0.23	0.09	0.08	0.06	0.07	0.10	0.09	0.10	0.16	0.17
Cl	0.08	0.36	0.81	0.52	0.25	0.16	0.08	0.69	0.04	0.04	0.51
P ₂ O ₅	0.12	0.08	0.11	0.18	0.10	0.13	0.21	0.33	0.15	0.22	0.10
TiO ₂	0.31	0.12	0.52	0.42	0.59	0.57	0.56	0.56	0.47	0.55	0.59
SUM	69.32	62.12	81.77	78.56	80.87	78.33	79.22	78.24	75.00	79.08	77.40

3.4. FTIR Analysis

FTIR spectra of the fine fraction of samples mostly corresponding to the binder are illustrated in Figure 5. Phase identification was performed by using standard literature and standard samples available in the database of laboratory [21,34,35].

The characteristic peaks of calcite are 1410, 872, and 710 cm⁻¹ [21]. Aragonite is identified by the peaks at 712 and 1082 cm⁻¹ [36,37]. The band at around 710 cm⁻¹ for the mortar samples was assigned to the deformation vibration of the C-O band in aragonite and calcite. The vibrations observed at 2512, 1417, 872, and 711 cm⁻¹ show the presence of dolomite. Si-O stretching vibrations observed at 787 and 464 cm⁻¹ are attributed to the presence of quartz and clay minerals. The peaks at 467, 1027, and 1630 cm⁻¹ are characteristic of the illite phase. The occurrence of bands at 1078, 1027, 726, and 690 cm⁻¹ support the presence of anorthite in the structure. The bands at 1085 and 1004 cm⁻¹ document the presence of corrensite, whereas the bands at 3620, 1006, 789, 464, and 422 cm⁻¹ indicate kaolinite. The characteristic peaks of vermiculite were obtained at 987 cm⁻¹ and 450 cm⁻¹. The vibrations obtained at 3649, 1042, 874, and 516 cm⁻¹ showed the presence of montmorillonite, whereas bands at 990, 788, 464, and 421 cm⁻¹ indicate albite [21]. The vibration band centered at approximately 455 cm⁻¹ is associated with the Al-O bonds that originate from the aluminosilicates [21].

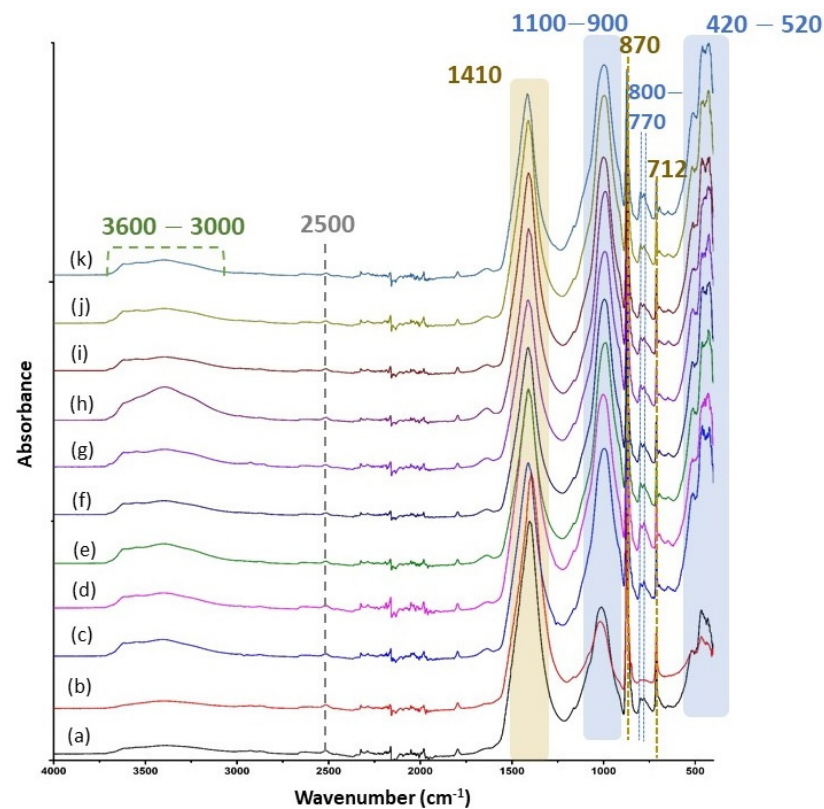


Figure 5. FTIR analysis results of the fine fraction (<63 μm) of samples (a) KM1, (b) KM5, (c) KM6, (d) KM10, (e) KM29, (f) KM31, (g) KM32, (h) KM34, (i) KM42, (j) KM47 and (k) local clay.

The FTIR results are helpful in identifying various forms of minerals present in the structure and confirm the results of XRD analysis. Because the fine fraction was analyzed, the identification of clay through FTIR is a cost-effective alternative in clay analysis that overcomes the laborious and non-environmentally friendly procedures involved in the dissolution of clays in organic solvents [38].

4. Conclusions

The analysis of mortar samples with stereomicroscopy, XRD, XRF, and FTIR shows that the samples are mainly composed of calcite and silicates in major quantities along with aluminum, magnesium, and iron oxide in minor quantities. A wide variety of local aggregates and ceramic fragments were used in the production of these ancient mortars. The high calcitic nature of the samples is attributed to the use of lime as a binder, along with earthen material and aggregates of a carbonaceous nature. More specifically, the local earthen material (KM clay) used in the production of mortars contains large amounts of calcite in its structure. Samples are divided into two groups; lime binder mortars and earthen binder mortars. The first group contains a high amount of lime, very fine grain sand (<0.5 mm), and fibers (straw), whereas the second group exhibits a high amount of earthen binder and sea sand with sea shells of varying quantities and size in the mortar matrix. The binder to aggregate ratio differed in the studied samples, ranging from 1/3 to 1/2. Lime lumps observed in a few samples indicate that either the binder was not homogeneously mixed with the aggregates or the binder was not slaked perfectly. This might be one of the main reasons of the poor preservation of the mortars. Other reasons for their poor state are aeolic, seismic, and hydrographic actions, as well as sulfate attacks that lead to efflorescence.

The design of the restoration mortars will be done according to the properties of the original ones. These new mortars need to be compatible with the original ones in terms of physical, chemical and mechanical properties. Therefore, high flexural strength, medium

modulus of elasticity, high water vapor permeability, low (or slow) water absorption, and high-water evaporation are necessary to avoid the water remaining on the mortars and the structures. The data obtained from this study will inform the design of new mortars that advance conservation goals of the master plan for the ancient port at Kommos in Crete.

Author Contributions: Conceptualization, P.-N.M. and J.W.; methodology, P.-N.M.; software, C.K.; validation, P.-N.M., C.K. and J.W.; formal analysis, M.B.U.; investigation, A.T.; resources, P.-N.M.; data curation, P.-N.M. and M.B.U.; writing—original draft preparation, M.B.U. and K.K.; writing—review and editing, P.-N.M. and J.W.; visualization, P.-N.M.; supervision, P.-N.M. and J.W.; project administration, P.-N.M.; funding acquisition, P.-N.M. and J.W. All authors have read and agreed to the published version of the manuscript.

Funding: This research was funded by Institute for Aegean Prehistory Study Center for East Crete INSTAP-SCEC S.A, Special Account of Research Funds (ELKE) project number 81350.

Institutional Review Board Statement: Not applicable.

Informed Consent Statement: Not applicable.

Data Availability Statement: Data available on request from the authors.

Acknowledgments: We would like to express our thanks to the Institute for Aegean Prehistory (INSTAP) and to INSTAP–Study Center for East Crete, for their financial support and technical assistance. Special thanks are expressed to Joseph and Maria Shaw of the University of Toronto, the American School of Classical Studies, Eleni-Eva Toumbakari, Head of the Section of Studies on Ancient Monuments, Directorate for Restoration of Ancient Monuments, and Vasiliki Sithiakaki, Ephorate of Antiquities of Heraklion for their kind collaboration.

Conflicts of Interest: The authors declare no conflict of interest.

References

1. Shaw, J.W. Excavations at Kommos (Crete) during 1979. *Hesperia* **1980**, *49*, 207–250. [[CrossRef](#)]
2. Shaw, J.W.; Shaw, M.C. *Kommos: An excavation on the South Coast of Crete, Volume 1, Part 1: The Kommos Region and Houses of the Minoan Town. Part 2. The Kommos Region, Ecology and Minoan Industries*; Princeton University Press: Princeton, NJ, USA, 2014.
3. Betancourt, P.P. *Kommos: An Excavation on the South Coast of Crete, Volume 2: The Final Neolithic through Middle Minoan Pottery*; Princeton University Press: Princeton, NJ, USA, 1992.
4. Shaw, J.W. *Kommos: A Minoan Harbour Town and Greek Sanctuary in Southern Crete*; American School of Classical Studies at Athens: Soudias, Athina, 2006; ISBN 0876616600/978-0876616604.
5. Shaw, J.W. Excavations at Kommos (Crete) during 1976. *Hesperia* **1977**, *46*, 199–240. [[CrossRef](#)]
6. Shaw, J.W. Excavations at Kommos (Crete) during 1978. *Hesperia* **1979**, *48*, 145–173. [[CrossRef](#)]
7. Shaw, J.W. Excavations at Kommos (Crete) during 1980. *Hesperia* **1981**, *50*, 211–251. [[CrossRef](#)]
8. Shaw, J.W. Excavations at Kommos (Crete) during 1981. *Hesperia* **1982**, *51*, 164–195. [[CrossRef](#)]
9. Shaw, J.W. Excavations at Kommos (Crete) during 1982–1983. *Hesperia* **1984**, *53*, 251–287. [[CrossRef](#)]
10. Shaw, J.W. Excavations at Kommos (Crete) during 1984–1985. *Hesperia* **1986**, *55*, 219–269. [[CrossRef](#)]
11. Moropoulou, A.; Bakolas, A.; Moundoulas, P.; Aggelakopoulou, E.; Anagnostopoulou, S. Optimization of compatible restoration mortars for the earthquake protection of Hagia Sophia. *J. Cult. Herit.* **2013**, *14*, e147–e152. [[CrossRef](#)]
12. Van Balen, K.; Papayianni, I.; Van Hees, R.; Binda, L.; Waldum, A. RILEM TC 167-COM: ‘Characterization of Old Mortars with Respect to their Repair’ Introduction to requirements for and functions and properties of repair mortars. *Mater. Struct.* **2005**, *38*, 781–785. [[CrossRef](#)]
13. Schueremans, L.; Cizer, Ö.; Janssens, E.; Serré, G.; Van Balen, K. Characterization of repair mortars for the assessment of their compatibility in restoration projects: Research and practice. *Constr. Build. Mater.* **2011**, *25*, 4338–4350. [[CrossRef](#)]
14. Loureiro, A.M.S.; da Paz, S.P.A.; Veiga, M.R.; Angélica, R.S. Investigation of historical mortars from Belém do Pará, Northern Brazil. *Constr. Build. Mater.* **2020**, *233*, 117284. [[CrossRef](#)]
15. Aggelakopoulou, E.; Bakolas, A.; Moropoulou, A. Properties of lime-metakolin mortars for the restoration of historic masonries. *Appl. Clay Sci.* **2011**, *53*, 15–19. [[CrossRef](#)]
16. Moropoulou, A.; Bakolas, A.; Moudoulas, P.; Aggelakopoulou, E. Reverse Engineering: A proper methodology for compatible restoration of mortars. In *Proceedings of the Workshop Repair Mortars for Historic Masonry, Delft, The Netherlands, 26–28 January 2005*; RILEM Publications SARL: Delft, The Netherlands, 2009; pp. 278–291.
17. Pacheco-Torgal, F.; Faria, S.; Jalali, S. Some considerations about the use of lime-cement mortars for building conservation purposes in Portugal: A reprehensible option or a lesser evil? *Constr. Build. Mater.* **2012**, *30*, 488–494. [[CrossRef](#)]

18. Moropoulou, A.; Bakolas, A.; Moundoulas, P.; Aggelakopoulou, E.; Anagnostopoulou, S. Strength development and lime reaction in mortars for repairing historic masonries. *Cem. Concr. Compos.* **2005**, *27*, 289–294. [[CrossRef](#)]
19. Biscontin, G.; Bakolas, A.; Moropoulou, A.; Zendri, E. Microstructural characterization of the historical mortars in Venice. In *Proceedings of the 3rd International Symposium on the Conservation of Monuments in the Mediterranean Basin, Venice, Italy, 22–25 June 1994*; pp. 405–410.
20. Biscontin, G.; Bakolas, A.; Maravelaki, P.; Zendri, E. Microstructural and composition characteristics of historic mortars in Venice. In *Proceedings of the Conservation of Stone and Other Materials. Conference Proceedings. Volume 1. Rilem-Unesco, Paris, France, 29 June–1 July 1993*; Thiel, M.J., Ed.; Chapman and Hall: Paris, France, 1993; pp. 178–185.
21. Farmer, V.C. *Infrared Spectra of Minerals*; Mineralogical Society: London, UK, 1974.
22. Maravelaki-Kalaitzaki, P.; Galanos, A.; Doganis, I.; Kallithrakas-Kontos, N. Physico-chemical characterization of mortars as a tool in studying specific hydraulic components: Application to the study of ancient Naxos aqueduct. *Appl. Phys. A* **2011**, *104*, 335–348. [[CrossRef](#)]
23. Artioli, G.; Secco, M.; Addis, A. The Vitruvian legacy: Mortars and binders before and after the Roman world. *EMU Notes Mineral* **2019**, *20*, 151–202.
24. Moropoulou, A.; Bakolas, A.; Bisbikou, K. Investigation of the technology of historic mortars. *J. Cult. Herit.* **2000**, *1*, 45–58. [[CrossRef](#)]
25. Regev, L.; Poduska, K.M.; Addadi, L.; Weiner, S.; Boaretto, E. Distinguishing between calcites formed by different mechanisms using infrared spectrometry: Archaeological applications. *J. Archaeol. Sci.* **2010**, *37*, 3022–3029. [[CrossRef](#)]
26. Chu, V.; Regev, L.; Weiner, S.; Boaretto, E. Differentiating between anthropogenic calcite in plaster, ash and natural calcite using infrared spectroscopy: Implications in archaeology. *J. Archaeol. Sci.* **2008**, *35*, 905–911. [[CrossRef](#)]
27. Weiner, S. *Microarchaeology: Beyond the Visible Archaeological Record*; Cambridge University Press: Cambridge, UK, 2010.
28. Reeder, R.J. *Carbonates: Mineralogy and Chemistry*; Mineralogical Soc. of America: Washington, DC, USA, 1990.
29. Corti, C.; Rampazzi, L.; Bugini, R.; Sansonetti, A.; Biraghi, M.; Castelletti, L.; Nobile, I.; Orsenigo, C. Thermal Analysis and archaeological chronology: The ancient mortars of the site of Baradello (Como, Italy). *Thermochim. Acta* **2013**, *572*, 71–84. [[CrossRef](#)]
30. Suzuki, M.D.; Dauphin, Y.; Addadia, L.; Weiner, S. Atomic order of aragonite crystals formed by mollusks. *CrystEngComm* **2011**, *13*, 6780–6786. [[CrossRef](#)]
31. Mayer, B.Y. *Archaeomalacology: Molluscs in Former Environments of Human Behaviour*; Oxbow Books: Oxford, UK, 2005.
32. Riquelme, F.; Alvarado-Ortega, J.; Cuevas-Garcia, M.; Ruvalcaba-Sil, J.L.; Linares-Lopez, C. Calcareous fossil inclusions and rock-source of Maya lime plaster from the Temple of the Inscriptions. Palenque, Mexico. *J. Archaeol. Sci.* **2012**, *39*, 624–639. [[CrossRef](#)]
33. Moropoulou, A.; Bakolas, A.; Michailidis, P.; Chronopoulos, M.; Spanos, C.H. Traditional technologies in Crete providing mortars with effective mechanical properties. *Trans. Built Environ.* **1995**, *15*, 11.
34. Genestar, C.; Pons, C.; Más, A. Analytical characterisation of ancient mortars from the archaeological Roman city of Pollentia (Balearic Islands, Spain). *Anal. Chim. Acta* **2006**, *557*, 373–379. [[CrossRef](#)]
35. Biscontin, G.; Birelli, M.P.; Zendri, E. Characterization of binders employed in the manufacture of Venetian historical mortars. *J. Cult. Herit.* **2002**, *3*, 31–37. [[CrossRef](#)]
36. Singh, M.; Kumar, S.V.; Waghmare, S.A.; Sabale, P.D. Aragonite–vaterite–calcite: Polymorphs of CaCO₃ in 7th century CE lime plasters of Alampur group of temples India. *Constr. Build. Mater.* **2016**, *112*, 386–397. [[CrossRef](#)]
37. Toffolo, M.B.; Regev, L.; Dubernet, S.; Lefrais, Y.; Boaretto, E. FTIR-Based Crystallinity Assessment of Aragonite-Calcite Mixtures in Archaeological Lime Binders Altered by Diagenesis. *Minerals* **2019**, *9*, 121. [[CrossRef](#)]
38. Kaufhold, S.; Hein, M.; Dohrmann, R.; Ufer, K. Quantification of the mineralogical composition of clays using FTIR spectroscopy. *Vib. Spectrosc.* **2012**, *59*, 29–39. [[CrossRef](#)]